SPRAY COMBUSTION CHARACTERISTICS OF PALM BIODIESEL

Cheng Tung Chong[1,2,*] and Simone Hochgreb[2]
*Email: ctc31@cam.ac.uk
[1] Faculty of Mechanical Engineering, Universiti Teknologi Malaysia 81310 Skudai, Johor, Malaysia.
[2] Hopkinson Lab, Department of Engineering, University of Cambridge, Trumpington Street, CB2 1PZ Cambridge, UK.

Abstract

The potential of Palm Methyl Esters (PME) as an alternative fuel for gas turbines is investigated using a swirl burner. The main air flow is preheated to 623 K and a swirling spray flame is established at atmospheric pressure. The spray combustion characteristics of PME are compared to diesel and Jet-A1 fuel under the same burner power output of 6 kW. Investigation of the fuel atomizing characteristics using Phase Doppler Anemometry (PDA) shows that most droplets are distributed within the flame reaction zone region. PME droplets exhibit higher Sauter Mean Diameter (SMD) values than baseline fuels, and thus higher droplet penetration length and longer evaporation timescales. PME swirl flame presents a different visible flame reaction zone while combusting with low luminosity and produces no soot. NOx emissions per unit energy are also reduced by using PME relative to those of conventional fuels, in spite of the ~17% higher specific fuel consumption and slightly larger droplets.

1. Introduction

Concerns about the rising fuel price and global climate change have led to the search for alternative fuels and energy sources. Biodiesel is recognized as a viable substitute for diesel fuel. The growing importance of biodiesel is shown through the increasing annual productions and blending mandates implemented in various countries [1]. Biodiesel can be produced from vegetable and animal oils through a transesterification process, in which the triglycerides from vegetable oils react with methanol to form methyl esters and glycerol. Depending on the feedstock, the biodiesel produced typically consists of a mixture of several methyl esters [2]. The physical properties of biodiesel are comparable to those of diesel, albeit with lower heating values. For this reason, biodiesel can be used neat or as blend with diesel in compression ignition engines. It was reported that biodiesel is able to reproduce the desired efficiency as diesel fuel but with higher fuel specific consumption. Lower emissions of soot, CO, CO_2 but higher NOx were achieved by using biodiesel [3].

Although biodiesel is mainly used in diesel blends in compression-ignition engines, application in gas turbine engines or furnaces for power generation is further envisaged. The feasibility of using biodiesels in gas turbines has been shown in field tests. Molière *et al.* [4] demonstrated that NOx emission of rapeseed biodiesel is lower compared to diesel fuel in a 40 MW gas turbine. The emissions of CO and NO for soy, palm biodiesel and 20% biodiesel blend with diesel are reported to be similar in a semi-closed cycle gas turbine field test [5]. Implementation of emission mitigation measures requires detailed understanding of the combustion characteristics of different fuels.

Krishna [6] examined the emissions of soy biodiesel and blends of soy biodiesel with diesel fuel in a 30 kW micro gas turbine engine (Capstone C30) test. The result showed reduction of CO and NO emissions for biodiesel and blends and no loss of thermal efficiency. However, Bolszo and McDonell [7] reported an increase of NOx emissions when soy

biodiesel was used instead of diesel, but that improved NOx emissions could be achieved by increasing the mass ratio of the atomizing air to liquid fuel. The conflicting result shows that more in depth investigation of biodiesel combustion is needed.

There have been a few combustion tests on biodiesel conducted using swirl burners. Sequera *et al.* [8] investigated the emissions of diesel, soy methyl ester, soy ethyl ester and bio-oil pyrolised from hardwood. Their results demonstrated that biodiesel blended fuels emitted lower NOx and CO at conditions where the fuel flow rates are kept constant. Similar trends of emission reduction using biodiesel were observed in experiments conducted by Panchasara *et al.* [9]. It was reported that the reduction of NO emission of biodiesel is associated with the lower flame temperature that is achieved with the increase of atomizing air. Hashimoto *et al.* [10] investigated the emissions of palm biodiesel relative to diesel in a gas turbine type burner. The result indicates that NO emission for palm biodiesel is consistently lower compared to diesel fuel when plotted as a function of excess air ratio, droplet SMD, atomizing air pressure and viscosity. These results indicate that biodiesel produces lower NOx emission than diesel fuel under gas turbine conditions, contrary to the higher NOx emissions measured in compression-ignition engine experiments [11, 12].

In this paper, the combustion characteristics of palm biodiesel are investigated under the swirling spray flame conditions using PDA and flame imaging technique. The data obtained can be used as a validation targets for biodiesel swirl flame modeling as well as practical combustor or injector design. The emission performance of the PME relative to baseline fuels is also investigated.

2. Experimental

2.1 Burner and flow delivery

The swirl burner in this experiment consists of a circular quartz tube forming the combustor wall and a swirler at the burner outlet. The axial swirler consists of eight straight vanes fixed at the angle of 45^{o} which generate strong swirl intensity. The swirl number, S_N is calculated as 0.78 based on the equation $S_N=2/3(1-(D_h/D_s)^3/(1-(D_h/D_s)^2))\tan\theta$, where D_h and D_s represent the swirler hub diameter and the swirler diameter respectively, and θ is the angle of the swirl blade from the centreline [13]. A plain-jet airblast atomizer (Delavan: SN type-30610-1) is placed concentrically with the swirler. The diameters of the air and fuel orifice are 1.7 mm and 0.5 mm respectively. The swirl vanes and airblast nozzle are flush mounted to the burner face as shown in Fig. 1a. The swirler is held by a central tube designed for delivering atomizing air and liquid to the atomizer. The liquid spray generated from the atomizer is enveloped by the swirling air coaxially. The atomizing air and fuel flows are independently controlled. The fuel flow rate is accurately supplied to the atomizer via a Bronkhorst® Coriolis mass flow controllers (M13 mini CORI-FLOW®), with an accuracy of ± 0.4%. The main air flow and atomizing air are separately regulated by two Bronkhorst® thermal mass flow controllers (MFC), which deliver the full scale accuracy of ± 1% respectively. The schematic of the single swirl flame burner configuration and flow delivery system is presented in Fig. 1b.

The main air flow is heated by two in-line air heaters (750 W/heater) arranged in series. The burner plenum and body are additionally heated by three Omega® rope heaters (500 W/rope) and insulated with high temperature heat-resisting materials to reduce heat loss. A 1.5 mm diameter thermocouple is placed 10 mm under the swirler to measure the temperature of the main air. The heating facility allows the main air to be preheated to a temperature of 350 ^{o}C. The signal from the thermocouple provides the feedback control to the temperature controller of the air heaters. The uncertainty of the temperature associated with the preheated air is within ± 5K. The whole burner is constructed using stainless steel.

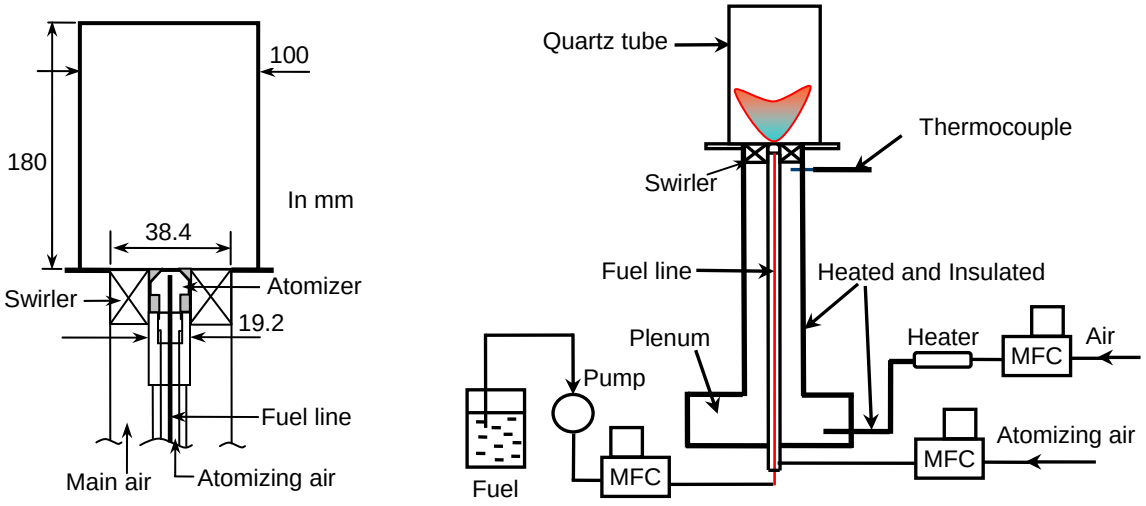

Figure 1: (a) Geometry of the swirl burner and (b) schematic of the flow delivery system.

2.2 Fuel

Table 1: Properties of Diesel, Jet-A1, PME

Properties	Jet-A1	Diesel	PME
Approx. formula	$C_{11}H_{21}$	$C_{16}H_{34}$	$C_{19}H_{36}O_2$
H/C ratio*	1.98	1.9	1.89
C/O ratio*	-	-	9.83
Spec. grav. 15^{o}C	0.81	0.85	0.88
Viscosity 40^{o}C (cSt)	-	2.6	4.5
Pour point (^{o}C)	-	-20	-18
Flash point (^{o}C)	38	60-72	174
Boiling range (^{o}C)	166-266	190-360	>215
LHV (kJ/kg)	43150	43090	36770
Cetane number	-	52	62.6

* Laboratory analysis

Biodiesel is typically composed of a mixture of methyl esters with no aromatic rings or sulphur. Due to the presence of oxygen in the molecules, biodiesels have lower heating values compared to conventional petroleum-fuels. The winter grade palm biodiesel/methyl esters (PME) used in this experiment is supplied by Carotino Sdn. Bhd. Malaysia. The PME conforms to the European Union's EN14214 standard with the approximated composition of 43.1% methyl oleate, 39.5% methyl palmitate, 10.4% methyl linoleate and 5% methyl stearate [14]. Jet-A1 fuel is a light distillate fuel that consists of a complex hydrocarbon mixtures of 50-65% paraffins, 10-20% aromatics and 20-30% naphtenes [15]. The standard Jet-A1 fuel used here is sourced from Conoco Limited, UK. Another conventional fuel tested here is diesel fuel. The present commercial grade low sulphur diesel fuel is obtained from the Shell petrol station in the UK. The typical composition of diesel fuel is 25-50% of paraffins, 20-40% of cycloparaffins and 15-40% of aromatics [16]. Comparison of the properties of biodiesel with conventional fuels is shown in Table 1. PME has higher density and viscosity compared to diesel. The low volatility of PME is reflected by the relatively high flash point of

174 ^{o}C. The ignition delay time of PME is shorter than diesel as indicated by the higher cetane number.

2.3 Operating conditions

The main bulk swirling air flow is preheated to a temperature of 350 ^{o}C while the liquid fuel and atomizing air are delivered to the atomizer at room temperature. The interaction of the swirling air flow with the liquid spray forms a globally lean mixture. To compare the combustion characteristics of the fuels, the flames are established at the same power output condition. The air and fuel mass flow rates are metered accordingly based on the fuels energy content to obtain the burner power output at 6 kW while maintaining the global equivalence ratio of ϕ=0.47. The atomizing air-to-fuel mass flow rate ratio (ALR) is set constant at 2.0 for all test cases. The operating conditions are shown in Table 2 for the respective fuels.

Table 2: Operating conditions

Fuel	Main air (g/s)	Fuel (g/s)	Atomizing air (g/s)	Global ϕ	Power (kW)
Diesel	4.15	0.14	0.28	0.47	6.0
Jet-A1	4.09	0.14	0.28	0.47	6.0
PME	4.04	0.16	0.32	0.47	6.0

2.4 Phase Doppler anemometry (PDA)

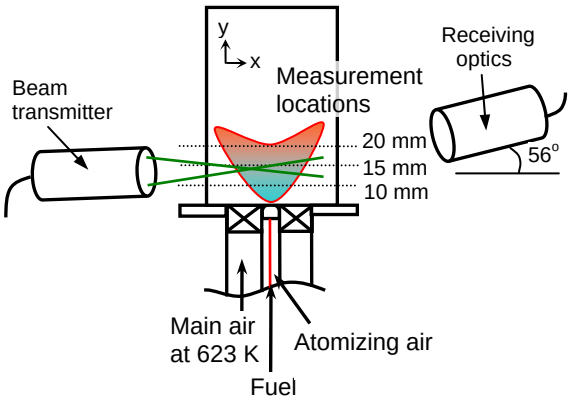

Figure 2: PDA setup and measurement locations.

Table 3: PDA optical setting

Transmitting optics	
Wavelength	514.5 nm
Power	0.8 W
Beam spacing	45 mm
Beam width	2.2 mm
Focal Length	500 mm
Number of fringes	26
Width of measurement vol.	0.149 mm
Length of measurement vol.	3.312 mm
Receiving Optics	
Focal length	310 mm
Scattering angle	56^{o}

The simultaneous measurement of droplets velocity and size is performed using a Phase Doppler Anemometry (PDA). The droplet size is determined based on the measured phase shift difference between two Doppler bursts, whereas the droplet velocity is obtained from the Doppler burst frequency [17]. The 1D PDA (Dantec 112 mm Fiber PDA) consists of a continuous-wave Argon-ion laser (Coherent: Innova 70C) that produces a laser beam at 514.5 nm. The beam from the laser is split into two almost identical beams via a beam splitter. A 500 mm focal lens is used to form a measurement volume at the intersection point of the beams. The receiving optics that houses the detectors are positioned at 56^{o} off axis to the transmitter to capture the light scattered from the droplets. Table 3 shows the beam

transmitter and the optical settings for the PDA system. Both the transmitting and receiving optics are mounted onto a 3-D traverse system with stepper motors that have the spatial accuracy of ±0.1 mm. The PDA measurement was performed within the flames established at the burner outlet. Measurements were taken at axial positions of 10, 15 and 20 mm downstream of the burner outlet as indicated in Fig. 2. Locations close to the spray outlet were not measured as the dense spray region may cause the PDA measurements to be unreliable. A minimum of 2000 data points were taken for each spatial point along the radial profiles. The statistical uncertainty is estimated to be 2% for the droplets velocity and diameters. Validation rates determined by the PDA software for the droplets velocity and sizes were at least 90%.

3. Results and discussion

3.1 Droplet velocity and SMD profiles

Measurements of the spray characteristics of reacting flows established from diesel, Jet-A1 and PME fuels were performed under fixed power conditions. The droplet velocity and SMD profiles on one side of the centreline are shown in Fig. 3 for 10, 15 and 20 mm from the burner outlet. The x-abscissa indicates the radial profile from the centreline (x= 0 mm) of the burner. At 10 mm from burner exit, the droplet velocity peaks at the radial position 3 mm as shown in Fig. 3a. The droplet axial velocity profile then decreases as the radial distance increases from the centreline. At further downstream location of 15 mm, the velocity peak appears at a wider radial distance as a result of the interaction of the spray with the main swirling flow as shown in Fig. 3b. The strong radial flow from the swirling flow induces a radial pressure gradient, in which the central recirculation zone is formed while the spray spreads radially. The strong reverse flow at the centreline region interacts with the droplets, which lowers the droplets velocity further downstream.

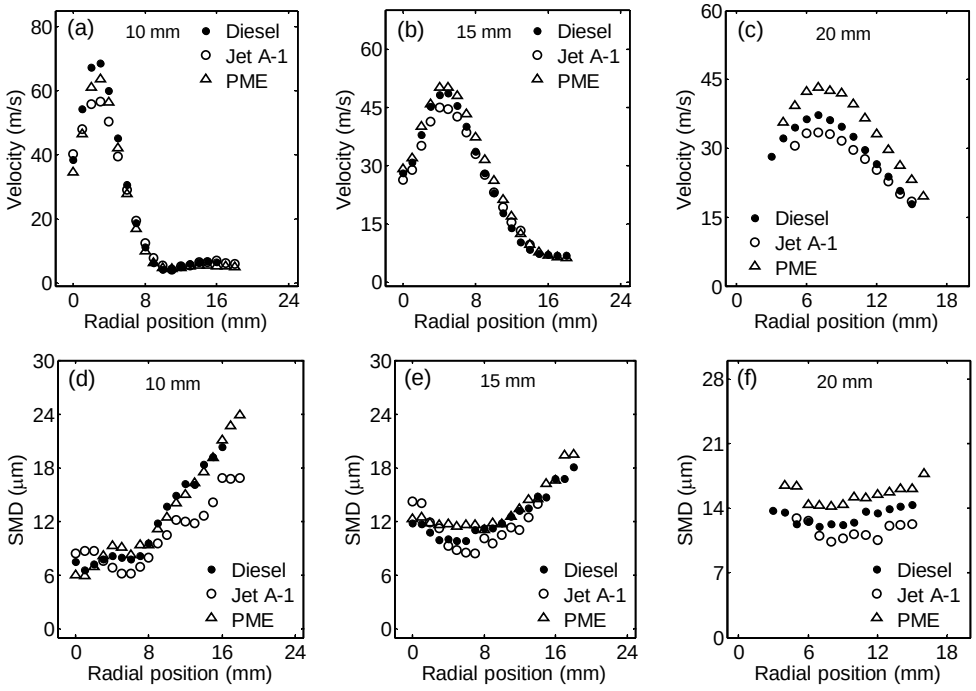

Figure 3: Droplet axial velocity (a,b,c) and SMD profiles (d,e,f) for diesel, Jet-A1 and PME flames established under constant power conditions for three different heights from the burner face.

Diesel exhibits similar velocity and SMD profiles as PME at locations 10 and 15 mm downstream the spray outlet. A low SMD values is observed at the centreline region but gradually increases with increasing radial positions. Between the radial position at 8 mm and the centreline, the droplets are distributed within the intense heat release region. The heat propagated from the reaction zone assists in vaporising the small droplets within this region. At the radial position of 5 mm, which coincides with the location of maximum volume flux, a slight increase of SMD values for diesel and PME is observed.

At the downstream location of 20 mm, the difference between droplet velocity and size becomes more obvious, as presented in Fig. 3c and 3f. PME droplets show higher SMD and velocity values than diesel droplets at the same spatial locations. The larger SMD value for PME droplets is due to the influence of higher viscosity and surface tension values compared to diesel fuel. The small and scarce droplets at the centreline and periphery region have completely vaporised whereas the high droplet density region sustains some larger droplets. The remaining large PME droplets contain higher momentum and thus enable longer penetration length with extended evaporation time.

Jet-A1 flame shows a slightly lower velocity and SMD values compared to diesel and PME fuels at all axial locations. This is because Jet-A1 fuel is more volatile and has lower boiling point value compared to the heavier hydrocarbons. Hence, droplet vaporisation occurs in a relatively shorter time scale due to the higher dispersion rate and smaller droplet size. The smaller droplets contain lower velocity due to the loss of momentum as the downstream axial distance increases.

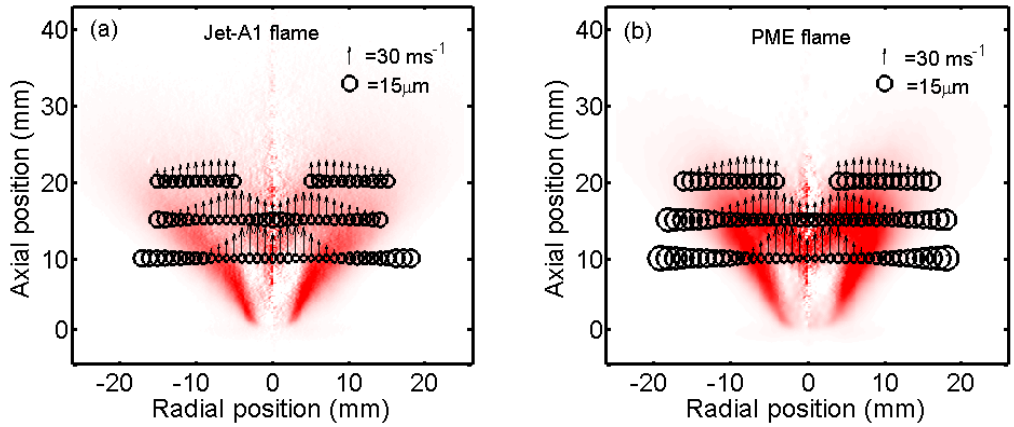

Figure 4: Droplet velocity and size distribution within the (a) Jet-A1 and (b) PME swirl flames superimposed on the corresponding CH* chemiluminescence signals.

The droplet size and axial velocity distribution superimposed on the mean CH* chemiluminescence intensity are shown in Fig 4a and 4b for Jet-A1 and PME flames. Despite the different shape of heat release zone shown by the CH* chemiluminescence signal, the overall droplet distribution is rather similar. Small droplets are distributed within the reaction zone while bigger droplets are located outside the flame zone. The intense heat within the flame facilitates evaporation of droplets. At the downstream location of 20 mm, droplets at the centre region are completely vaporised and no further CH* chemiluminescence is detectable. The larger droplets outside the flame zone appear at much lower velocity than the smaller droplets at the centre region of the flame. The high droplet velocity at the centreline region is attributed to the high momentum attained from the atomizing air. The PME flame shows an overall larger droplet distribution compared to Jet-A1 flame.

3.2 Droplet concentration and volume flux

The droplet number density and volume flux profiles of the spray flames at the axial location 10, 15 and 20 mm downstream of burner outlet are shown in Fig. 5. The distribution at all downstream axial locations indicates that droplet concentration peaks at a distance away from the centreline (x=0 mm). The PME flame presents higher peak droplet number density than diesel and Jet-A1 by a factor of 2 and 4 respectively, at the spatial radial position of 7 mm as shown in Fig. 5a. The high droplet density and volume flux is partly in due to the higher mass flow rates of PME by ~17% compared the baseline fuels under constant power condition. The remaining larger PME droplets that are not completely vaporised also contribute to the droplet density count. Jet-A1 fuel shows lower droplet number density and volume flux present in flame due to the high volatility of the fuel, which facilitates vaporisation.

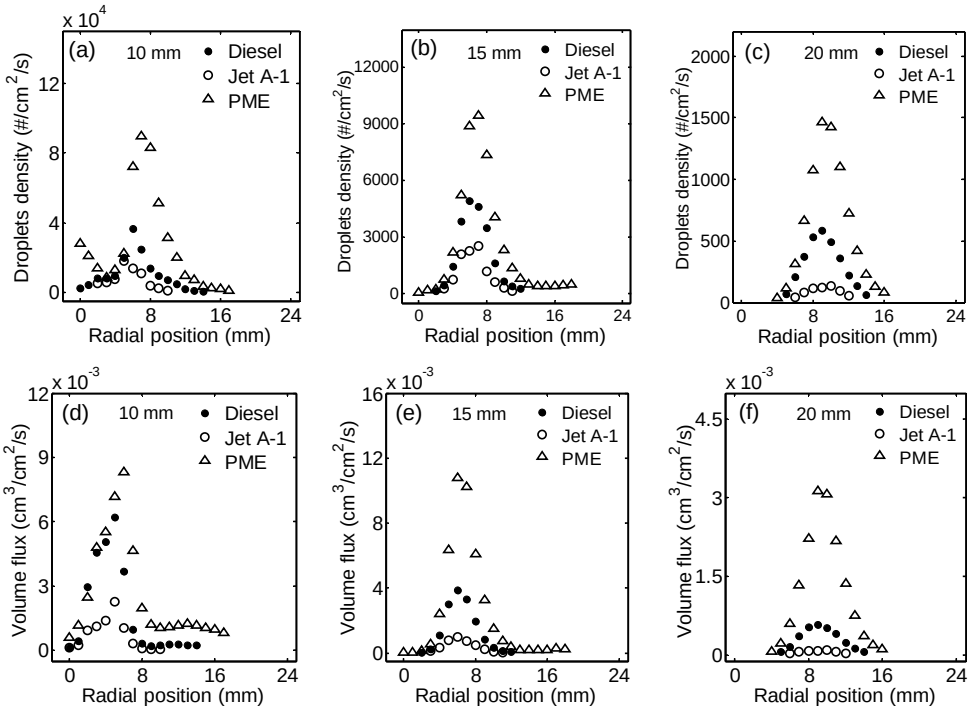

Figure 5: Droplet number density (a,b,c) and volume flux (d,e,f) profiles at axial locations 10, 15 and 20 mm from burner outlet under constant power conditions.

Despite the slight difference of droplet SMD profiles between diesel and PME (Fig. 3), the droplet concentration and volume flux is observed to be lower for diesel at all spatial locations. The droplet density peaks shifts from radial position 7 mm to 9 mm between downstream axial locations of 15 and 20 mm due to the radial spreading of the spray. In regions where the droplet number density is high, rapid mixing with air creates a leaner mixture for reactions. This is shown in Fig. 4 where the intense heat reaction zone corresponds to the locations where the droplets density peaks. Away from the flame zone (x>10 mm), the droplets exhibit larger SMD values but the droplet number density and volume flux distribution in these regions are very low as shown in Fig. 5. The CH* chemiluminescence intensity peaks at locations where the droplet density is high but with relatively small droplets. This suggests that the variation of the spray droplet distribution and concentration has significant influence on the flame shape and reaction zone.

3.3 Flame imaging

The global flame structure of liquid swirl flames were imaged via line-of-sight CH* chemiluminescence (430±10 nm) and broadband spectrum (>550 nm) using an intensified CCD camera. The obtained line-of-sight images were averaged (300 images) and deconvoluted via Abel transformation to obtain the planar flame structures. The excited CH* chemiluminescence from the flames can be used as an indicator of heat release rate [18]. Figure 6a, 6b and 6c show the planar flame structures of Jet-A1, diesel and PME swirl flames respectively. The Jet-A1 flame exhibits the heat release zone of similar shape to diesel but with a slightly wider flame angle. The PME flame presents a more locally intense joint flame front. The high intensity of the CH* emission for PME could be due to the late vaporisation of droplets and higher localized diffusion flames.

The length of all the flame reaction zones is approximately 30 mm downstream of the burner outlet. This demonstrates that the highest local flame temperature occurs in a relatively similar spatial region within the combustor. Complete vaporisation and consumption of droplets occur within this region despite the difference in fuel source. The corresponding CH* intensity profiles at 4, 8, 13 and 17 mm from the burner outlet are presented in Fig. 7a, 7b and 7c respectively. Jet-A1 flame shows similar CH* intensity profiles at 13 and 17 mm as diesel flame but with lower intensity peaks at profiles of 4 and 8 mm. The PME flame shows similar intensity profiles at 4 and 8 mm as Jet-A1, but higher intensity at 13 and 17 mm compared to both Jet-A1 and diesel flames. The intense localized heat near the flame root as shown in diesel flame may assist in flame stabilization near the burner outlet.

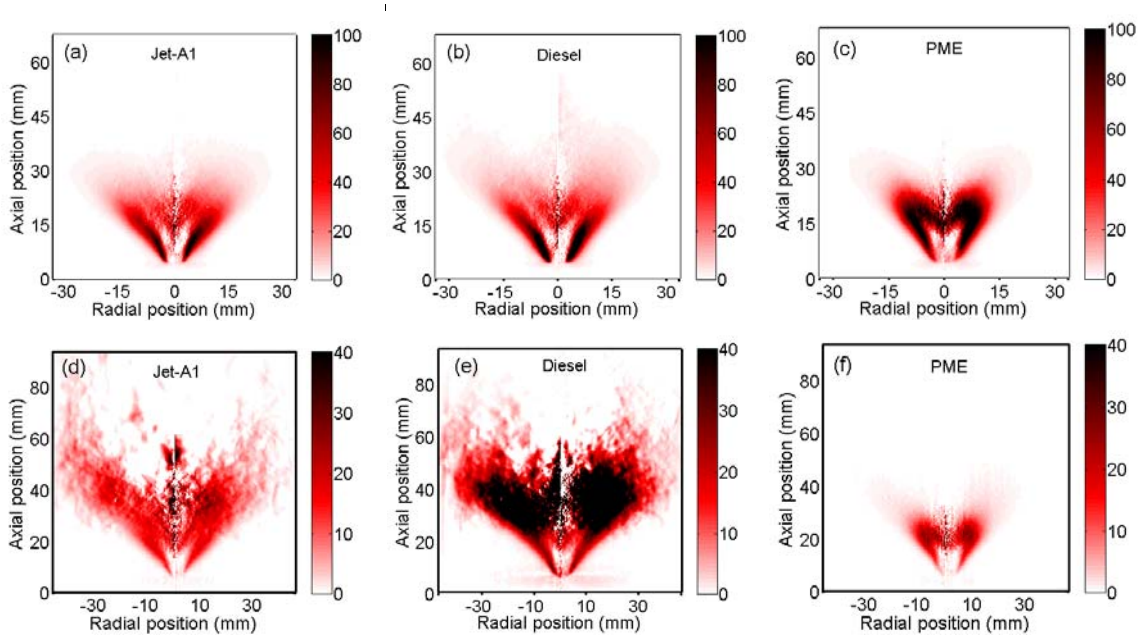

Figure 6: Abel transformed CH* chemiluminescence (a,b,c) and longpass filtered (>550 nm) imaging (d,e,f). The intensity of the signals is shown in the bar next to each image.

As most of the thermal energy intensity of the flame is distributed in the continuous spectra of 550 nm and beyond, a CCD camera coupled with a broadband longpass filter is used to image the region where soot is present. The longpass filtered images of Jet-A1, diesel and PME are presented in Fig. 6d, 6e and 6f respectively. Jet-A1 and diesel flames present a sooty region downstream of the reaction flame zone, but the latter shows much higher intensity than the former due to the high sooting tendency. From observation, both fuels

establish a bluish flame near the burner outlet (where the intense heat release occurs) and a luminous yellow flame downstream. The bluish premixed flame near the flame root is the typical characteristics of twin-fluid atomizer where the atomizing air enhances mixing with droplets [19]. The intense luminosity is attributed to the soot radiation as a result of high content of aromatic rings in diesel (~20-40%) and Jet-A1 fuel (~10-20%). It is also expected that the high soot radiation intensity of diesel flame increases the temperature of the downstream post combustion region.

In contrast, the PME flame exhibits no sign of soot within the combustor. The flame shows only the bluish region equivalent to a premixed flame. The image shown in Fig. 6f shows the intensity is mainly emitted from the heat release zone. The low luminosity of the palm biodiesel flame has also been observed by Hashimoto et al. [10] in a swirling flame investigation established using a pressure-swirl nozzle. The presence of oxygen in palm biodiesel enhances the local premixed combustion of hydrocarbon with oxygen whereas the absence of aromatic rings inhibits the formation of soot and the sooty yellowish flame brush downstream. It has also been reported that the soot generated from biodiesel is rapidly oxidised due to the initial incorporation of oxygen groups in the molecule [20].

The intensity profiles of longpass signals (>550 nm) at 12, 22, 30 and 40 mm downstream of burner outlet are shown in Fig 7d, 7e and 7f for Jet-A1, diesel and PME flames respectively. The diesel flame shows higher flame intensity by a factor of three compared to Jet-A1 flame. The highest intensity is found to occur at the profile of 30 mm downstream of the burner exit for both flames whereas PME shows no sign of soot at this particular region. The only intense region in the PME flame (12 mm downstream) coincides with the reaction zone and the profile is similar to those shown in Jet-A1 flame at the same spatial location.

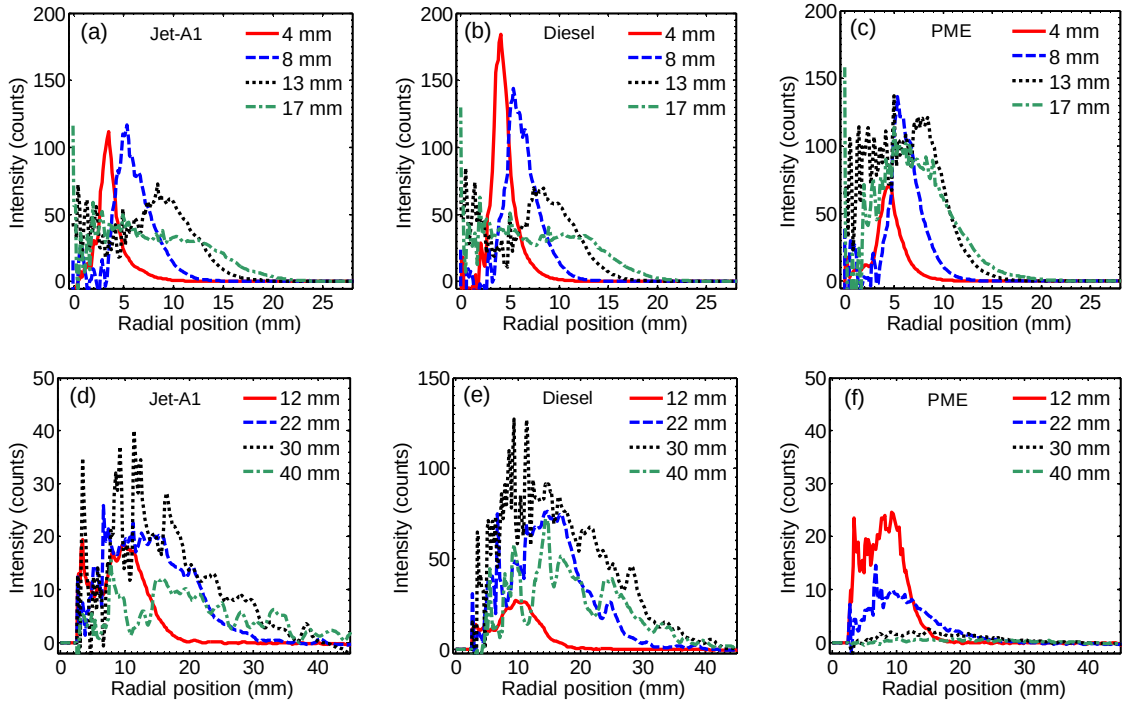

Figure 7: Intensity profiles of CH* chemiluminescence (a,b,c) and longpass filtered (>550 nm) signals (d,e,f) for Jet-A1, diesel and PME swirl flames under constant power conditions.

3.4 Flame spectroscopy

Flame emission spectroscopy was performed by spectrally resolving the flame spectrum into UV and near-infrared range (~200 – 900 nm). The global flame spectrum signal was focused onto the slit of a spectrometer (USB2000+; Ocean Optics) via a focusing lens. Figure 8 shows the global flame spectra obtained from Jet-A1, diesel and PME swirl flame. Diesel flame shows a prominent bandwidth curve between 550 to 850 nm due to the intense luminosity radiated by the soot. The peak around visible wavelength of 600 nm indicates the colour spectrum of yellow-orange as observed in the flame. Jet-A1 flame shows a reduced intensity for the soot band by half compared to diesel flame. The obtained flame spectroscopy concurs with the spatially-resolved long bandpass (>550 nm) filtered images as shown in Fig. 6 where the soot formation for Jet-A1 flame is lower than diesel flame. The PME flame is characterised as soot-free based on the near-zero intensity between the wavelength band of 580 and 900 nm. Comparison of the flame spectrum highlights the differences in the spectroscopy between conventional fuels and biodiesel which could be utilised as an optical sensing method.

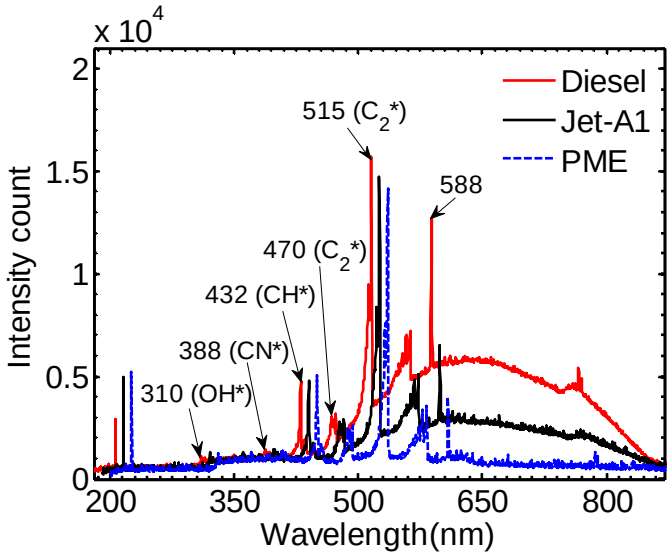

Figure 8: Flame emission spectroscopy measurements under constant power conditions. The spectra of Jet-A1 and PME are displaced along the wavelength axis by +10, +20 nm respectively for clarity.

3.5 Emission measurements

The post-combustion emissions of CO, NO and NO_2 were measured using a Tocsin 320® gas analyzer at the combustor outlet. A sampling probe of 4 mm in diameter was placed 10 mm inward from the burner exit to sample across the burner outlet. The averaged emissions values were obtained from 5 equally spaced positions with 2 minutes of sampling time for each spatial location. The sampling line was preheated to 180 ^{o}C and insulated to prevent condensation of post-combustion products.

Due to the variation of power density between the fuels, scaling to same power output and fuel/air mass ratio yields the global equivalence ratio of 0.47, 0.47 and 0.4 for diesel, Jet-A1 and PME flames respectively. The atomizing air to liquid ratio was maintained at 2.0 for all test cases. The emission results of NO, NO_2 and CO obtained as a function of power output is shown in Fig. 9.

Overall, PME flame shows a reduction of NOx emissions compared to diesel and Jet-A1 fuels. The reduction of NOx using PME fuel under the spray flame condition has also been reported by Hashimoto *et al*. [10]. Diesel and Jet-A1 flames exhibit relatively similar

NO, NO_2 and CO emissions. The main factor of lower NO_x emission by PME is attributed to the absence of nitrogen-bound component in the fuel. PME contains no aromatic ring and the flame is characterised by near-zero soot as shown in the longpass filtered (>550 nm) signals in Fig. 6f. The NO emission exhibits a decreasing trend as the power output increases as shown in Fig. 9a. The reduction of NO at higher power output could be due to the influence of the flow field, where the increased strength of the recirculation zone under higher air flow rates could affect the local flame temperature and mixedness and hence the formation of NO. NO_2 is present at an order of magnitude lower than NO. NO_2 shows a slight decrease with the increase of power output. A slight increasing trend is observed in CO emission.

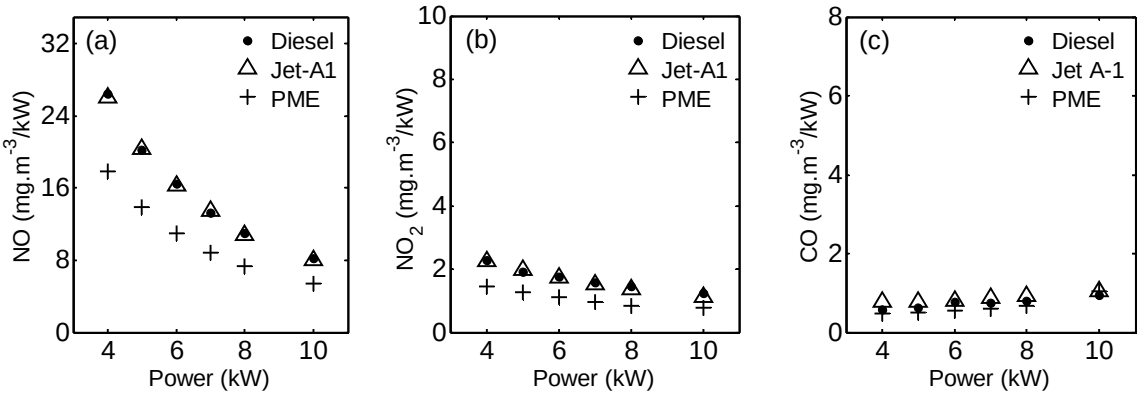

Figure 9: Specific emissions of (a) NO, (b) NO_2 and (c) CO as a function of burner power output.

4. Conclusions

The spray combustion characteristics of PME have been compared to diesel and Jet-A1 flames under the same power output condition. The droplets within the reacting flames are characterised using a PDA system. The interaction of the recirculation flow and the droplets causes the lower droplet velocity at the centreline region. Flame reaction zone tends to occur at spatial positions where the droplets density and volume flux are high. PME droplets show slightly higher SMD values than baseline fuels with higher droplets concentration and volume flux. The swirl flame generated from PME shows a bluish, low luminosity flame without the yellow sooty region. From CH* chemiluminescence imaging, the PME flame shows a more intense localized heat release region than flames established from conventional fuels. Longpass filtered (>550 nm) imaging shows no sign of soot for PME swirl flame, as supported by the spectrally resolved flame spectra. The emission result indicates that PME produces lower NOx under the overall lean mixture, continuous, swirling spray flame conditions.

Acknowledgements

The financial support from the Ministry of Science, Technology and Innovation (MOSTI) Malaysia (project number: 03-01-06-KHAS01) is gratefully acknowledged. The author would like to thank Prof. Gyung-Min Choi from Pusan National University for fruitful discussions.

5. References

[1] REN21., "Renewables 2010 global status report," REN21 Secretariat, Paris (2010).

[2] J. Van Gerpen, B. Shanks, R. Pruszko, D. Clements, and G. Knothe, "Biodiesel Production Technology," *NREL/SR-510-36244*, (2004).

[3] J. Xue, T. E. Grift, and A. C. Hansen, "Effect of biodiesel on engine performances and emissions," *Renew. Sust. Energy Rev.*, 15: 1098-1116, (2011).

[4] M. Molière, E. Panarotto, M. Aboujaib, J. M. Bisseaud, A. Campbell, J. Citeno, P. Maire, and L. Ducrest, "Gas turbine in alternative fuel applications: biodiesel field test," in *ASME Turbo Expo 2007: Power for land, sea, and air*, Montreal, Canada, 2007, pp. Paper no. GT2007-27212 pp. 397-406.

[5] W. Ellis, W. Lear, B. Singh, A. Srinivasan, J. Crittenden, and S. Sherif, "Flameless combustion of biofuels in a semi-closed cycle gas turbine," in *46th AIAA Aerospace Sciences Meeting and Exhibit*, Reno, Nevada, 2008.

[6] C. R. Krishna, "Performance of the capstone C30 microturbine on biodiesel blends," Brookhaven National Laboratory (2007).

[7] C. D. Bolszo and V. G. McDonell, "Emissions optimization of a biodiesel fired gas turbine," *Proc. Comb. Inst.*, 32: 2949-2956, (2009).

[8] D. Sequera, A. K. Agrawal, S. K. Spear, and D. T. Daly, "Combustion performance of liquid biofuels in a swirl-stabilized burner," *J. Eng. Gas Turbines Power*, 130: 032810.1-032810.10, (2008).

[9] H. V. Panchasara, B. M. Simmons, A. K. Agrawal, S. K. Spear, and D. T. Daly, "Combustion Performance of Biodiesel and Diesel-Vegetable Oil Blends in a Simulated Gas Turbine Burner," *J. Eng. Gas Turbines Power*, 131: 031503.1-031503.11, (2009).

[10] N. Hashimoto, Y. Ozawa, N. Mori, I. Yuri, and T. Hisamatsu, "Fundamental combustion characteristics of palm methyl ester (PME) as alternative fuel for gas turbines," *Fuel*, 87: 3373-3378, (2008).

[11] M. N. Nabi, M. S. Akhter, and M. M. Zaglul Shahadat, "Improvement of engine emissions with conventional diesel fuel and diesel-biodiesel blends," *Bioresour. Technol.*, 97: 372-378, (2006).

[12] M. Canakci, "Combustion characteristics of a turbocharged DI compression ignition engine fueled with petroleum diesel fuels and biodiesel," *Bioresour. Technol.*, 98: 1167-1175, (2007).

[13] J. M. Beer and N. A. Chigier, "Combustion aerodynamics," *Appl. Sci. Publ. London*, (1972).

[14] A. Gopinath, S. Puhan, and G. Nagarajan, "Relating the cetane number of biodiesel fuels to their fatty acid composition: a critical study," *Proc. of the Inst. of Mech. Eng., Part D: J. Automobile Eng.*, 223: 565-583, (2009).

[15] P. Dagaut, A. El Bakali, and A. Ristori, "The combustion of kerosene: Experimental results and kinetic modelling using 1- to 3-component surrogate model fuels," *Fuel*, 85: 944-956, (2006).

[16] J. T. Farrell, N. P. Cernansky, F. L. Dryer, D. G. Friend, C. A. Hergart, C. K. Law, R. M. McDavid, C. J. Mueller, A. K. Patel, and H. Pitsch, "Development of an Experimental Database and Kinetic Models for Surrogate Diesel Fuels," *SAE Paper 2007-01-0201*, 2007 SAE World Congress: 16-19 April 2007, (2007).

[17] F. Durst and M. Zare, "Laser Doppler measurements in two-phase flows," in *Proceedings LDA-Symposium Copenhagen*, Copenhagen, Denmark, 1975, pp. 403-429.

[18] Y. Hardalupas and M. Orain, "Local measurements of the time-dependent heat release rate and equivalence ratio using chemiluminescent emission from a flame," *Combust. Flame*, 139: 188-207, (2004).

[19] A. H. Lefebvre, "Airblast atomization," *Prog. Energy Combust. Sci.*, 6: 233-261, (1980).

[20] J. Song, M. Alam, A. L. Boehman, and U. Kim, "Examination of the oxidation behaviour of biodiesel soot," *Combust. Flame*, 146: 589-604, (2006).